Mechanisms of Sarcomere Assembly in Muscle Cells Inferred from Sequential Ordering of Myofibril Components

Francine Kolley [1], Clara Sidor [2], Benoit Dehapiot [2,3], Frank Schnorrer [2,*] and Benjamin M. Friedrich [1,†]

[1]*Physics of Life, TU Dresden, 01307 Dresden, Germany*
[2]*Aix Marseille University, CNRS, IBDM, Turing Centre for Living Systems, 13288 Marseille, France*
[3]*ScopeM, ETH Zurich, 8093 Zurich, Switzerland*

Voluntary movement in animals is driven by the contraction of myofibrils in striated muscle cells, which are linear chains of regular cytoskeletal units termed sarcomeres. While the ordered structure of mature sarcomeres, key to muscle contraction, is well established, the physical mechanism governing sarcomere assembly is still under debate. Here we put forward a theory of sarcomere self-assembly based on data. We measured the sequential ordering of sarcomere components in developing *Drosophila* flight muscles, using a novel tracking-free algorithm. We find that myosin molecular motors, α-actinin cross-linkers, and the titin homologue Sallimus form periodic patterns before actin filaments become polarity sorted. Based on these, we propose that myosin, Sallimus, and sarcomere Z-disk proteins including α-actinin dynamically bind and unbind to an unordered bundle of actin to establish an initial periodic pattern. Periodicity of actin filaments is established only later. Our model proposes that nonlocal interactions between spatially extended myosin and titin/Sallimus containing complexes, and possibly tension-dependent feedback mediated by an α-actinin catch bond, drive this ordering process. We probe this hypothesis using mathematical models and derive predictive conditions for sarcomere pattern formation to guide future experiments.

I. INTRODUCTION

Striated muscle as well as heart muscle cells contain acto-myosin bundles of almost crystalline regularity, termed myofibrils, which span the entire multinucleated muscle cell with a length of up to several millimeters [1]. Activation of myosin activity results in the contraction of myofibrils [2,3], which powers all voluntary movements in humans and animals, as well as heartbeat. Each myofibril is a periodic chain of stereotypic units, termed sarcomeres, with a well-defined, micrometer-range length. Each sarcomere is bordered by two α-actinin-rich Z-disks, which cross-link parallel, polarity-sorted actin filaments at their plus ends (barbed ends); see also Fig. 1(a), right. Actin filament minus ends face towards central, bipolar myosin filaments, cross-linked by myomesin (or Obscurin in *Drosophila*). Importantly, the giant protein titin (Sallimus in *Drosophila*), anchored at the Z-disk, stably links actin (thin filaments) and bipolar myosin filaments (thick filaments) together by extending from the Z-disk to the center of the sarcomere in mammals [4] or to the beginning of myosin filaments in insect flight muscles [5]. Sarcomeres

self-assemble during muscle development [1,6,7], and defects in sarcomere assembly result in severe myopathies [8,9].

Despite many years of research on sarcomere and myofibril development, we still do not understand the physical mechanisms that drive this self-assembly process in developing muscle or heart cells. In particular, it remains open why mechanical tension is essential for sarcomere formation *in vivo* and *in vitro* [6,7,10–12], prompting for physical descriptions. Sanger and colleagues proposed in the premyofibril hypothesis that nonmuscle myosin and Z-disk proteins establish early periodic patterns, with nonmuscle myosin being replaced by muscle-myosin later [13]. This model may apply in some muscles; however, the periodicity of nonmuscle myosin is not always clearly visible [7,14]. Irrespective of whether early myofibrils comprise nonmuscle or only muscle-specific myosin filaments, the key question is the following: how do the first periodic patterns form?

Holtzer and colleagues observed small I-Z-I bodies comprising Z-protein aggregates, as well as free-floating stacks of bipolar myosin filaments in atypical myogenic cells [15], leading to the proposal that these "building blocks" may become stitched together at later stages to form sarcomeres. Latent protein complexes were also proposed as precursors for *Drosophila* larval muscles [16] or chicken cardiomyocytes [17]. However, it is not clear how such large supramolecular complexes could move in the crowded environment of a muscle cell.

Previous mathematical models commonly assumed that periodic patterns of polarity-sorted actin filaments form simultaneously with periodic patterns of myosin and Z-disk

---

*Corresponding author: frank.schnorrer@univ-amu.fr
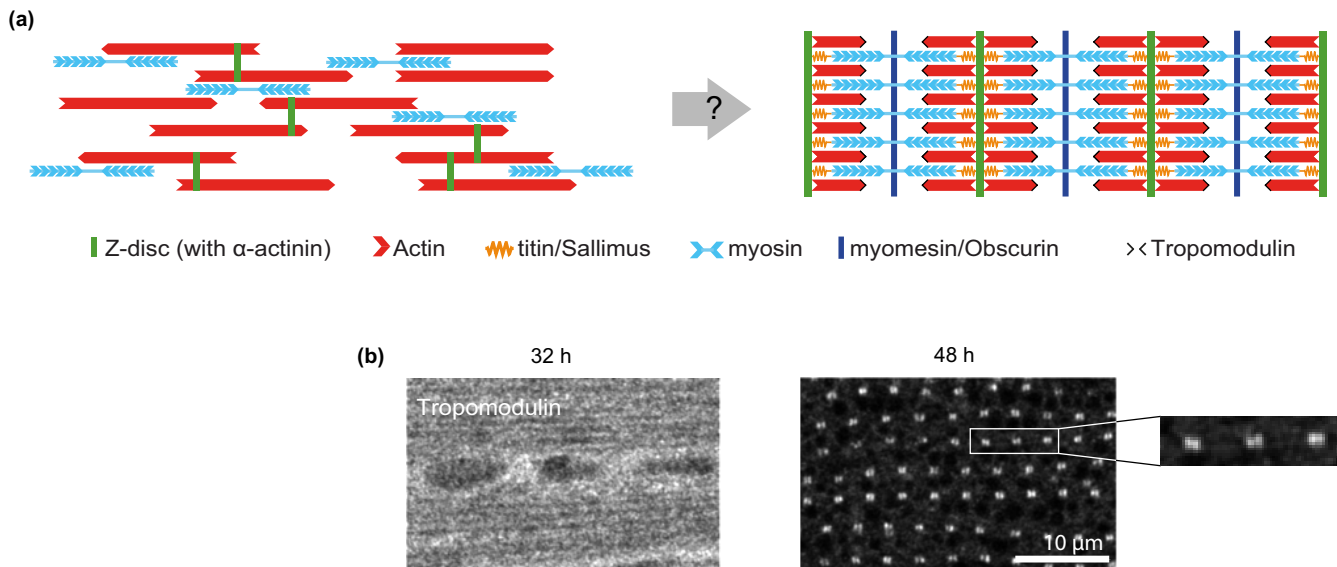†Corresponding author: benjamin.m.friedrich@tu-dresden.de

FIG. 1. (a) Myofibrillogenesis represents a pattern formation problem: how do initially stress-fiber-like bundles of parallel actin filaments (red) with homogeneous distribution of myosin (blue) and Z-disk proteins (green) rearrange into periodic sarcomeric patterns? In mature myofibrils, actin filaments form polarity-sorted domains, with their plus ends cross-linked at the Z-disk rich in α-actinin, which marks the boundary of the sarcomere. Bipolar myosin filaments in the middle of each sarcomere are cross-linked by myomesin/Obscurin (dark blue) and anchored to the Z-disks by titin/Sallimus (yellow). (b) Images of *Drosophila* flight muscle at 32 h and 48 h APF showing tropomodulin (Tmod), which specifically binds to actin filaments minus ends (pointed end), using an endogenous GFP-Tmod line [76,77]. Tmod is detectable at 32 h APF, but does not display periodic patterns yet. At 48 h APF, periodic patterns of Tmod indicate polarity sorting of actin filaments, delineating the boundaries of the H-zone. Scale bar 10 μm.

proteins [18–20]. Zemel *et al.* showed how a hypothetical second, minus-end directed molecular motor could establish periodic cytoskeletal patterns [18,21]. Yoshinaga *et al.* showed how a generic coupling between actin polarity and stress fields result in the same pattern [19]. Finally, Friedrich *et al.* proposed actin polymerization forces as a physical mechanism for the polarity sorting of actin filaments into a periodic pattern [20]. None of these theoretical mechanisms have been confirmed by experimental data so far, and some mechanisms pose open questions, for example, actin polymerization forces may be too weak to drive filament sorting [22,23]. Furthermore, titin, which was shown to be indispensable for myofibril assembly [24–26] and proposed to directly affect sarcomere length [4,27–29], had not been included in these previous models. More generally, theoretical descriptions of cytoskeletal pattern formation in pure acto-myosin systems predict localization of myosin filaments near the plus end of actin filaments [30,31], which is opposite to their localization in mature sarcomeres [see Fig. 1(a), right].

Here quantifications of periodic patterns in assembling myofibrils of *Drosophila* muscles lead us to propose a new model: our data suggest that myosin and Z-disk proteins establish the first periodic patterns, while actin forms a polarity-sorted pattern only later. We postulate that myosin and Z-disk proteins bind and unbind to a bundle of actin filaments, which are aligned in parallel or antiparallel, and thus are not yet polarity sorted [Fig. 1(a), left]. Reciprocal interactions between myosin and Z-disk proteins, possibly mediated indirectly through titin, favor the formation of periodic sarcomeric patterns. Only subsequently will actin become polarity sorted, possibly by preferential nucleation of actin filaments at emergent periodically positioned

Z-bodies, and gradual depolymerization of ectopic actin filaments.

We additionally introduce a second, modified model based on mechanical tension generated by myosin motor activity. We show that the proposed catch-bond behavior of the Z-disk protein α-actinin [32–35] is sufficient to drive the formation of periodic patterns in simulations, thus providing a mechanistic underpinning for the idea that effective elastic interactions between myosin bipolar filaments may drive sarcomeric pattern formation [36].

II. RESULTS

A. Polarity sorting of actin filaments

In *Drosophila melanogaster*, myofibrillogenesis is a multi-stage process, in which sarcomere assembly starts after 22 h after puparium formation (APF). Previous work has shown that unstriated bundles of nematically aligned actin filaments form at 22 h APF [37]. These bundles contain actin filaments that are aligned parallel or antiparallel to the bundle axis. Yet no apparent actin polarity sorting or periodic patterns are visible at that stage, as schematically sketched in Fig. 1(a). These unstriated acto-myosin bundles develop into myofibrils with periodic sarcomeric patterns visible by 32 h APF [6,37,38]. We have verified that the polarity sorting of actin filaments occurs rather late during sarcomere assembly, as the minus-end actin-capping protein Tropomodulin (Tmod) is detectable at 32 h, yet is still homogeneously distributed along developing myofibrils. At 48 h APF, characteristic patterns of Tmod become visible, marking the actin filament minus ends at the boundaries of the H-zone [Fig. 1(b)]. Thus, actin filaments are nematically ordered at the beginning of

sarcomeric pattern formation and polarity sorted in mature myofibrils.

B. Sequential emergence of periodic patterns during myofibrillogenesis

To gain insight into the gradual establishment of periodic sarcomeric patterns in developing myofibrils, we obtained multichannel fluorescence z-stack images of dorsal longitudinal flight muscles (DLMs) from *Drosophila melanogaster* stained for α-actinin, actin, myosin, and the titin homologue Sallimus (Sls) at selected time points; see Fig. 2(a).

No periodic patterns are observable by eye at 22 h and 24 h APF. At 26 h, the first periodic patterns with alternating localization of α-actinin, Sallimus, and myosin start to emerge. Actin, however, does not yet display obvious periodic patterns at 26 h. Over time, periodic patterns become increasingly pronounced and are clearly visible for all four sarcomere components at 32 h [Fig. 2(a)]. Thus, sarcomere proteins assemble into periodic patterns from 26 h to 32 h APF.

C. A robust, tracking-free algorithm to compute correlations functions

To quantify the order of individual proteins in these micrographs, we developed a tracking-free image-analysis algorithm to compute correlation functions of protein intensities along myofibrils [Fig. 2(b); see also Fig. S1 in the Supplemental Material (SM) [39]]. This algorithm does not track individual myofibrils but uses the estimated local direction of myofibrils. Even manual tracking of individual myofibrils is impossible at early stages because myofibrils have not formed yet. Specifically, after preprocessing, a steerable filter was used to determine the local nematic direction of the Sallimus channel [Fig. 2(b)]. Next, intensity profiles $I(x)$ were computed for each channel from 5 μm line scans along these local nematic directions for each region of interest (ROI). Autocorrelation functions (ACFs) and cross-correlation functions (CCFs) were then computed from these intensity profiles and averaged over all ROIs; see the SM [39] for details.

D. Correlation functions reveal temporal order of sarcomeric components and suggest interactions

We computed autocorrelation functions for α-actinin, myosin, Sallimus, and actin at three selected time points [Fig. 2(c); for additional time points, see the SM [39]]. A Fourier peak at a position Δx in the ACF reveals periodic patterns with characteristic periodicity Δx, even if patterns are noisy. More precisely, a Fourier peak at position Δx of amplitude A indicates periodic order with periodicity $L \approx \Delta x$. In contrast, a random localization of a protein without any periodic pattern is reflected by a monotonically decreasing ACF. We applied this method to developing flight muscle images. At 22 h and 24 h APF, the ACFs display no evidence for periodic patterns for any of the four proteins (actin, myosin, Sls, α-actinin) tested [Fig. 2(c)]. A first indication for periodic patterns of α-actinin, Sallimus and myosin is found at 26 h APF as a small Fourier peak located at $\Delta x \approx 1.5$ μm [Fig. 2(c)]. The slightly larger peak of α-actinin suggests an initially more disperse distribution of myosin and Sallimus.

The amplitude of these Fourier peaks increases with time, reflecting the formation of increasingly regular patterns. The position of the Fourier peaks shift to $\Delta x \approx 2.1$ μm at 32 h APF, confirming the known increase of sarcomere size during the beginning of *Drosophila* myofibrillogenesis [38].

This length increase could result from myosin filaments growing in length [15], or mechanical tension that stretches sarcomeres, which was found to be high at this stage [40]. In contrast, the ACF for actin is still monotonically decreasing up to 30 h APF and shows only a Fourier peak at 32 h APF [Fig. 2(c)]. This observation strongly suggests that myosin, α-actinin and Sallimus form periodic patterns first, while actin follows 6 h later.

In addition to ACFs, we can compute cross-correlation functions (CCF) between different channels. As an example, Fig. 2(d) displays the CCF between the Sallimus N-terminus and myosin.

While a positive peak at $\Delta x = 0$ would indicate a *colocalization* between both proteins, a negative peak at $\Delta x = 0$, in contrast, indicates *local exclusion* of both proteins. The negative peak at $\Delta x = 0$ at 26 h APF in the Sallimus versus myosin CCF thus demonstrates an early anticorrelation between Sallimus N-terminus and myosin filaments, in which a locally elevated Sallimus signal implies a lower myosin signal at the same position and *vice versa* (see also Fig. S2 in the SM [39]). This observation is consistent with the hypothesis of a local negative interaction between Sallimus and myosin filaments. The observed local exclusion of Sallimus N-terminus and myosin precedes their alternating localization in mature myofibrils, where Sallimus N-terminus localizes near Z-disks at sarcomere boundaries, whereas myosin is located at the center of sarcomeres [26].

To assess possible spatial variations in myofibril maturation within the same muscle fiber, we also selected image regions with the most progressed myofibrillogenesis, which gave almost identical results with a maximal time shift of 2 h (Fig. S7 in the SM [39]) This demonstrates the high synchronization of pattern formation during sarcomere self-assembly.

In conclusion, our experimental data show that myosin and the titin-homologue Sallimus, which links Z-disk components to myosin, assemble into a periodic pattern before actin does. This assembly is largely homogeneous throughout the large muscle cells. At 24 h APF, small irregularities are already observable before a global periodic pattern emerges at 26 h APF.

E. A new mechanistic hypothesis

Based on previous work [6,37,38] and our observations from early stages of myofibrillogenesis in *Drosophila* flight muscle, we put forward two putative mechanisms that suggest how the self-organized formation of sarcomeres may happen. In both proposed mechanisms, myofibrillogenesis starts from initially unstriated bundles of nematically aligned actin filaments that are not polarity sorted yet, but are nematically ordered, i.e., aligned parallel or antiparallel to the bundle axis, resembling stress fibers in connective tissue cells. Myosin, Z-disk proteins (e.g., α-actinin) and Sallimus dynamically bind and unbind from these bundles, interacting in such a manner that regular patterns with alternating localization
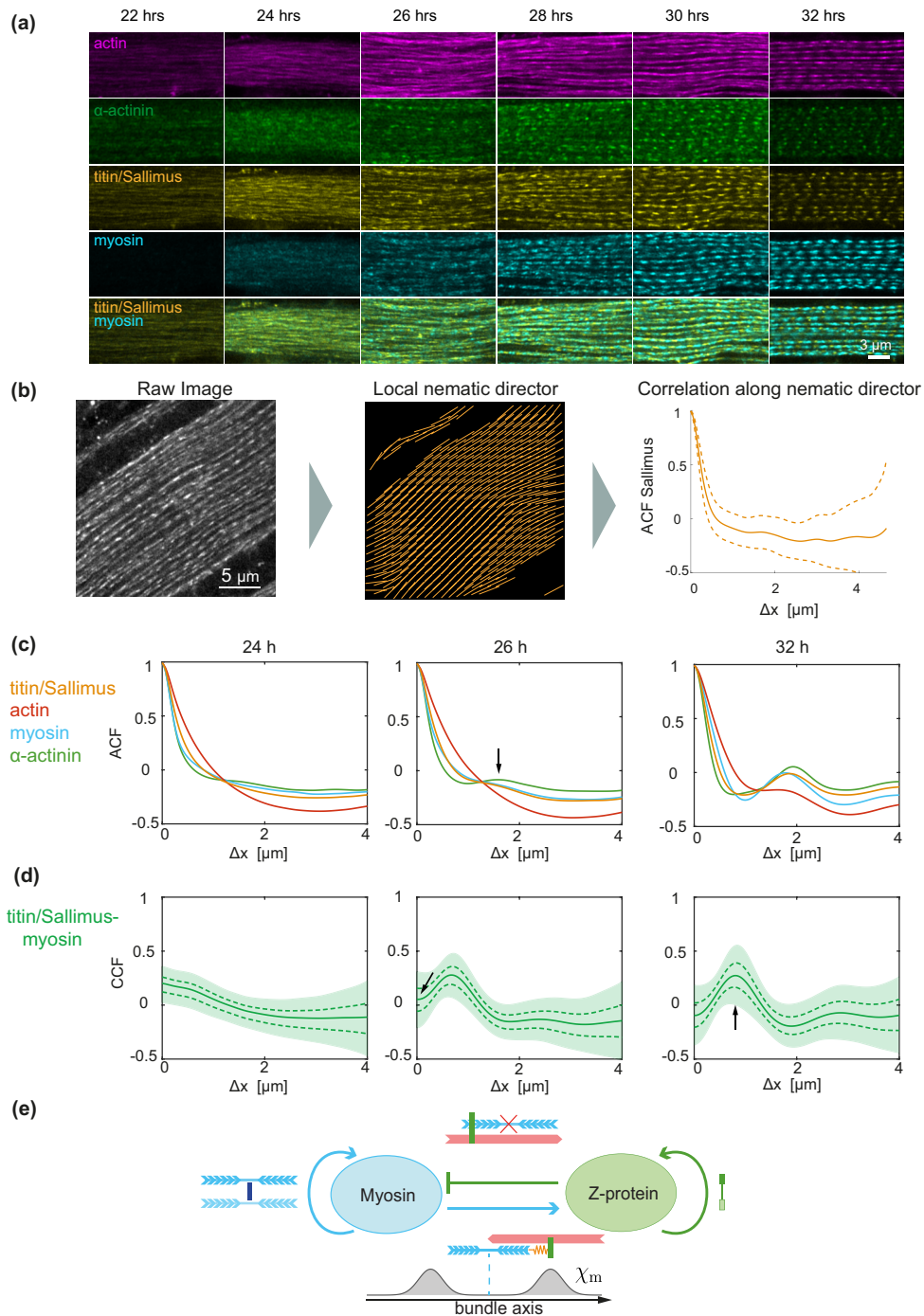
FIG. 2. (a) Multichannel images of *Drosophila* flight muscle at 22 h to 32 h after puparium formation (APF) with actin (magenta), myosin (blue), titin/Sallimus (yellow), and myosin-Sallimus merge. Scale bar 5 μm. (b) Tracking-free algorithm to compute correlation functions along local bundle axis. After preprocessing, a field of local nematic directors is determined (middle). Line scans along these nematic directions enable to compute mean correlation functions (right). (c) Autocorrelation functions (ACFs) for actin (red), myosin (blue), Sallimus (yellow), and α-actinin (green) at selected time points. A monotonically decreasing ACF indicates a random distribution of proteins, while a peak (arrow) reveals periodic patterns with wavelength given by peak position. (d) Cross-correlation function (CCF) between myosin and Sallimus [green, mean $\pm$ s.e.m. (dashed), $\pm$ s.d. (shaded)]. A positive peak at nonzero Δx indicates a localization of the two proteins at a characteristic distance, while a negative dip at $\Delta x = 0$ indicates a local exclusion. (e) Proposed model of nonlocal interactions between myosin and Z-disk proteins driving pattern formation. Lateral interactions between bipolar myosin filaments and cross-linkers favor autocatalytic attachment. Lateral interactions between bipolar myosin filaments favor autocatalytic binding of myosin to the actin bundle. Likewise, interactions between Z-disk proteins favor autocatalytic binding of Z-disk proteins. Steric repulsion by Z-disk proteins impedes myosin binding to the actin bundle, causing a negative feedback. Finally, myosin recruits Sallimus, which recruits Z-disk proteins such as α-actinin. This positive feedback is nonlocal, here modeled by an interaction kernel χ_m with mean interaction distance $l_m/2 + l_s$ set by the length l_m of myosin and l_s of the giant protein Sallimus.

and correct periodicity emerge. Periodic actin patterns will become established later, possibly driven by continuous actin turnover, preferential nucleation at nascent Z-disks (or the M-line [41]), and depolymerization of ectopic actin filaments; see the Discussion section.

We assume that bipolar myosin filaments bound to the initial actin scaffold will recruit more myosin, representing autocatalytic stacking or *in situ* polymerization of myosin. This assumption is warranted by the experimental observation that bipolar myosin filaments form ordered stacks (and that existing stacks can "catch" new myosin filaments), as observed in nonmuscle cells [42], human osteosarcoma cells [43], a homozygous actin mutant [44], and atypical myogenic cells [15]. Moreover, aligned myosin filaments become cross-linked by M-line proteins (e.g., myomesin or Obscurin in *Drosophila*) [45].

Spontaneous aggregation was also described for Z-disk proteins, characterized by Z-disk protein punctae that fuse into larger nascent Z-disks [46]. Similar Z-disk protein aggregates had been observed previously in Taxol-treated cells [15]. Together, these observations strongly suggest autocatalytic aggregation of Z-disk proteins.

Figure 2(e) summarizes these putative molecular interactions between myosin and Z-disk proteins bound to actin. In addition to autocatalytic attachment of both myosin and Z-disk proteins, we assume that Z-disk proteins locally inhibit myosin binding due to steric hindrance of the relatively long myosin filament, reflecting a competition between Z-disk proteins and myosin filaments for free space to bind actin. This creates a negative feedback loop [Fig. 2(e)]. Complementarily, we propose that myosin enhances the binding of Z-disk proteins, reflecting the recruitment of Sallimus by myosin, which then recruits Z-disk proteins such as α-actinin at its N-terminus. For this, we assume that Sallimus attains its extended configuration already at early stages of myofibrillogenesis [5].

We [Fig. 2(a)] and others have shown that the *Drosophila* titin/Sallimus is already incorporated in nascent myofibrils at early stages of myofibrillogenesis [38,47]. It is thus plausible to assume that titin/Sallimus mediates a nonlocal interaction between myosin and Z-disk proteins already during sarcomere formation. Hence, more myosin will via titin also recruit more Z-disk proteins. This increase in both proteins is also seen in developing flight muscle sarcomeres [38,47] and Fig. 2(b). Recent super-resolution data have shown that the extended confirmation of titin/Sallimus spans also from the Z-disk (Sls N-terminus) to the myosin filaments (Sls C-terminus) in flight muscles [5].

Importantly, interactions between the spatially extended molecules define nonlocal interactions spanning over a distance set by the lengths of myosin filaments and Sallimus molecules [mathematically modeled as an interaction kernel sketched in Fig. 2(e)]; see the SM for details [39].

Experimental data suggest that giant proteins such as titin act as molecular rulers that, directly or indirectly, orchestrate sarcomeric length control [4,27–29]. In particular, expression of shorter titin isoforms caused a decrease of mature sarcomere length [4,28,29].

Next, we formulate the model shown in Fig. 2(e) as a minimal mathematical model referred to as model I, and

demonstrate its capability to establish regular sarcomeric patterns using agent-based simulations.

F. Sarcomeric pattern formation by nonlocal interactions

We translated the minimal mathematical model I, which assumes molecular interactions between myosin and Z-disk proteins as proposed in Fig. 2(e), into a minimal mathematical model. The model couples the concentration $m(x)$ of bound myosin filaments and $z(x)$ of bound Z-disk proteins as a function of the bundle axis coordinate x through binding and unbinding rates that depend on the number of molecules already bound, while accounting for small random movements of bound myosin and Z-disk proteins along the fiber axis due to random forces, modeled as apparent diffusion with effective diffusion coefficient D:

$$\frac{\partial m}{\partial t} = D\nabla^2 m - \beta\, m$$
$$+ \beta\, m^* \exp\{\mu[m - z - (m - m^*)^2]\}, \tag{1}$$

$$\frac{\partial z}{\partial t} = D\nabla^2 z - \beta\, z$$
$$+ \beta\, z^* \exp\{\zeta\,[\alpha\,(m_\chi - m^*) + (z - z^*) - (z - z^*)^2]\}. \tag{2}$$

For simplicity, we assume equal effective diffusion coefficients $D = D_m = D_z$ and equal unbinding rates $\beta = \beta_m = \beta_z$, as well as equal steady-state concentrations $m^* = z^*$ for myosin and Z-disk proteins; see the SM [39] for a generalization. The concentration $m(x)$ refers to the midpoints of extended myosin filaments.

The binding rate of myosin in Eq. (1) is modulated from the base rate β depending on the concentrations $m(x)$ and $z(x)$ of myosin and Z-disk proteins already bound to account for the molecular interactions reviewed in Fig. 2(e). The proposed autocatalytic binding of myosin is encompassed by the exponential factor $\exp(\mu m)$, while the factor $\exp(-\mu z)$ represents negative feedback of bound Z-disk protein on myosin recruitment due to steric interactions. The quadratic term in the exponential captures saturation effects that limit deviations from the steady-state concentration m^*.

Equation (2) for $z(x)$ is similar, with the important difference that the factor $\exp(\zeta\alpha m_\chi)$ describes a nonlocal interaction between extended myosin filaments and Z-disk proteins, mediated by the giant protein Sallimus. The interaction length $l_\chi = l_m/2 + l_s$ is set by the lengths l_m and l_s of myosin filaments and Sallimus. The parameter α allows one to tune the strength of this nonlocal interaction.

A linear stability analysis of Eqs. (1) and (2) reveals parameter regimes, for which the homogeneous steady state with uniform concentration profiles of myosin and Z-disk proteins $m(x) \equiv m^*$ and $z(x) \equiv z^*$ is unstable, and small spatial inhomogeneities in concentrations become amplified. Indeed, agent-based simulations with mean-field interactions based on Eqs. (1) and (2) yield regular periodic patterns with alternating peaks of bound myosin and Z-disk proteins; see Fig. 3(b) for an example.

We can use these agent-based simulations to probe whether periodic patterns also form for a given finite number of interacting molecules, when small-number fluctuations
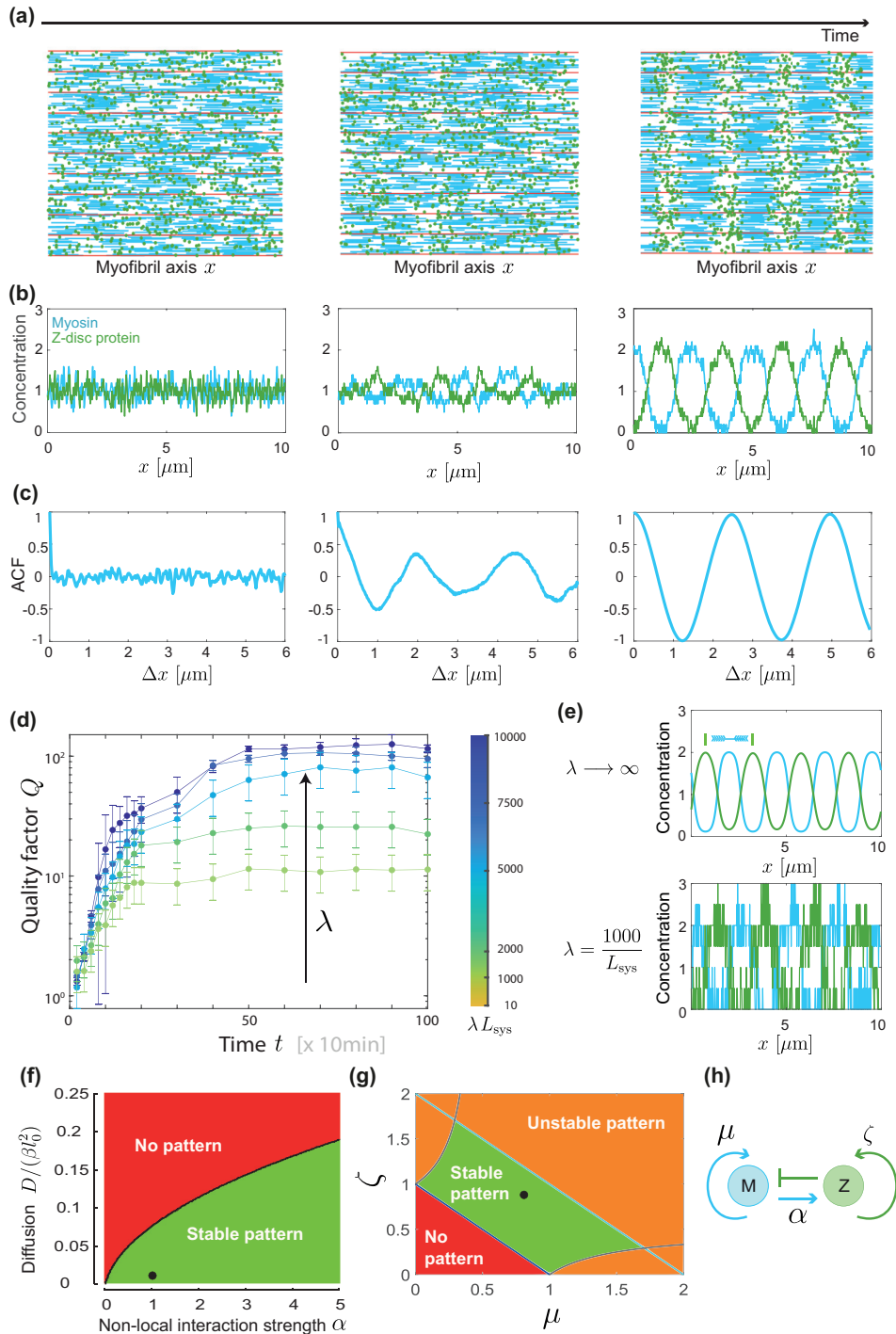
FIG. 3. Pattern formation by nonlocal interactions. (a) Agent-based simulations of mathematical model I as proposed in Fig. 2(e), simulated in one space dimension, visualized in two space dimensions, for different simulation times ($t = 0$, 2, 100) with myosin (blue) and Z-disk protein (green) bound to a scaffold of parallel, infinitely long actin filaments (shown schematically, red). (b) Corresponding concentration profiles at $t = 0$, 2, 100 for myosin (blue) and Z-disk protein (green). (c) Autocorrelation functions (ACFs) at $t = 0$, 2, 100 for myosin concentration. The ACF for $t = 0$ fluctuates around zero, reflecting the initially random distribution of myosin. The ACF for $t = 2$ exhibits a Fourier peak with amplitude A, indicative of a periodic pattern. (d) Quality factor $Q = -\pi / \ln(A)$ of periodic patterns determined from the amplitude A of the Fourier peak in the ACF of myosin concentration as function of time t for different values of total myosin density λ (mean $\pm$ s.e.m., $n = 10$ simulation runs). (e) Example concentration profile for different values of λ, corresponding to different steady-state values of the quality factor Q. A mean-field model was used for the limit $\lambda \to \infty$. (f) Phase diagram showing regimes of stable patten formation as function of the strength α of nonlocal interactions between myosin and Z-disk proteins, and the diffusion coefficient D of bound myosin filaments. (g) Analytical solution from linear stability analysis in the limit $D = 0$ reveals three different regimes as function of the autocatalytic feedback strengths μ and ζ. (h) Memo of interaction scheme highlighting parameters α, μ, ζ of Eqs. (1) and (2). Parameters (a–c): $\lambda = 5000/L_{\text{sys}}$. For detailed list of model parameters, see Table S1 in the SM [39].

perturb pattern formation. We introduce the total number of myosin filaments in the system as λL_{sys}. Changing the number-density parameter λ allows one to tune small-number fluctuations. The formal limit $\lambda \to \infty$ recovers the deterministic mean-field model (1)–(2). This model assumes effective mean-field interactions, in which each myosin filament and Z-disk protein interacts with all other molecules at the same location. This assumption is a valid approximation in a dense, three-dimensional acto-myosin bundle.

Figure 3(a) shows snapshots of agent-based simulation at different simulation times with $\lambda = 5000/L_{sys}$. At the start of the simulation ($t = 0$), myosin filaments and Z-disk proteins are randomly distributed. As the pattern evolves in time, stable periodic patterns form. The number of filaments M in a bin can be translated into a concentration by $m = M/(\lambda \Delta x)$; see Fig. 3(b). Analogous to the analysis of experimental data, we compute the autocorrelation function of myosin concentration; see Fig. 3(c). To quantify the regularity of simulated patterns, we define a quality factor $Q = -\pi / \ln(A)$ from the amplitude A of the first Fourier peak in these ACFs [48]; see Fig. 3(d). The quality factor Q increases with time and eventually saturates at a value Q_{max}, reflecting the emergence of a stable pattern. The mean quality factor at steady-state Q_{max} increases with increasing number-density parameter λ, reflecting the decreasing impact of small-number fluctuations. In the formal limit $\lambda \to \infty$, Q_{max} is expected to diverge to infinity as patterns become perfectly periodic; see Fig. 3(e).

We emphasize that the formation of periodic patterns in model I is driven by the nonlocal interaction between myosin and Z-disk proteins and does not emerge from a diffusion-driven instability as in classical Turing models [49]. Figure 3(f) shows a phase diagram of model I as a function of the nonlocal interaction strength α and the effective diffusion coefficient D, corroborating the fact that nonlocal interactions must outcompete the deleterious effects of diffusion to allow for the formation of periodic patterns. This remains true even if diffusion constants $D_m \neq D_z$ were different. In the limit $D \to 0$, we can derive analytical conditions for the feedback parameters ζ and μ to predict whether stable periodic patterns or no patterns or unstable patterns form; see Fig. 3(g).

The length of sarcomeres in simulated patterns depends approximately linearly on the interaction length scale of the nonlocal interactions, which is set by the length of myosin filaments and titin (Fig. S13 in the SM [39]). A partial knock-down of myosin or Z-disk proteins reduces the regularity of sarcomeric patterns and suppresses sarcomeric patterns beyond a characteristic knock-down strength (Fig. S14). A similar effect is predicted for a reduction of actin density (Fig. S15).

In conclusion, model I based on nonlocal interactions is capable of driving the spontaneous formation of periodic sarcomeric patterns and makes testable predictions.

G. Sarcomeric pattern formation by tension-responsive catch bonds

In addition to molecular interactions, mechanical tension was shown to be essential for sarcomere formation [6].

Myotubes are set under tension after they attach to tendon cells. Live-imaging in *Drosophila* revealed that periodic sarcomeric patterns emerge simultaneously across the entire length of initially unstriated muscle fibers, concomitantly with an increase in tissue mechanical tension. This suggests that the global level of mechanical tension in these fibers coordinates sarcomere assembly (concomitantly increasing nematic order and density of the actin filaments) [1,6,37]. In light of this global role of mechanical tension guiding sarcomere assembly, it is tempting to speculate that local, position-dependent tension within nascent sarcomeres may also stabilize molecular interactions by modulating rates of unbinding. In particular, binding of α-actinin to actin filaments has been recently shown to display catch-bond behavior at the cortex of HeLa cells [33,35] and in reconstituted actin networks [34].

To explore this hypothesis, we introduce a second model, in which myosin filaments bound to antiparallel actin filaments exert molecular tension on cross-linked Z-disk proteins; see Fig. 4(a). This provides an alternative nonlocal interaction of myosin filaments acting (indirectly) on Z-disk proteins. Together with the molecular interactions sketched in Fig. 2(e), this defines model II of tension-dependent pattern formation. We make the simplifying assumption that translocation of actin filaments within the cross-linked actin bundle of the nascent myofibril can be neglected.

In this model II, the structural polarity of actin filaments becomes important. In our one-dimensional model, there are two polarities of actin filaments, depending on whether their plus-end points to the left ($+$) or right ($-$), while length l_a is assumed constant. Correspondingly, we distinguish three different populations of myosin filaments bound to the scaffold of actin filaments; see Fig. 4(a).

We denote the concentrations of myosin filaments bound to actin filaments of only one polarity as $m_+(x)$ and $m_-(x)$, depending on actin polarity; see Fig. 4(a). These single-bound myosin filaments move to the plus end of actin with velocities $-v_0$ and $+v_0$, respectively.

Yet a third population of myosin filaments are bound to actin filaments of both polarities, whose concentration we denote by $m_2(x)$. These double-bound myosins do not move but generate local tension $\sigma(x)$ by pulling on actin filaments of opposite polarity. This local tension $\sigma(x)$ can be expressed as a function of the concentration of double-bound myosin filaments $m_2(x)$ using interaction kernels $\chi_\pm$ that characterize the expected overlap of actin and myosin filaments [see also Fig. 4(a)]:

$$\sigma = f_0(m_2 * \chi_- + m_2 * \chi_+). \tag{3}$$

To account for the tension-responsive catch-bond behavior of Z-disk proteins such as α-actinin [33–35], we assume that the unbinding rate β_z of Z-disk proteins decreases with increasing tension

$$\beta_z = \beta_{z,0} \exp(-\sigma/\sigma_c). \tag{4}$$

We can now formulate the minimal model II as a mean-field model that couples the concentrations of single-bound myosin $m_\pm(x)$, double-bound myosin $m_2(x)$, and Z-disk
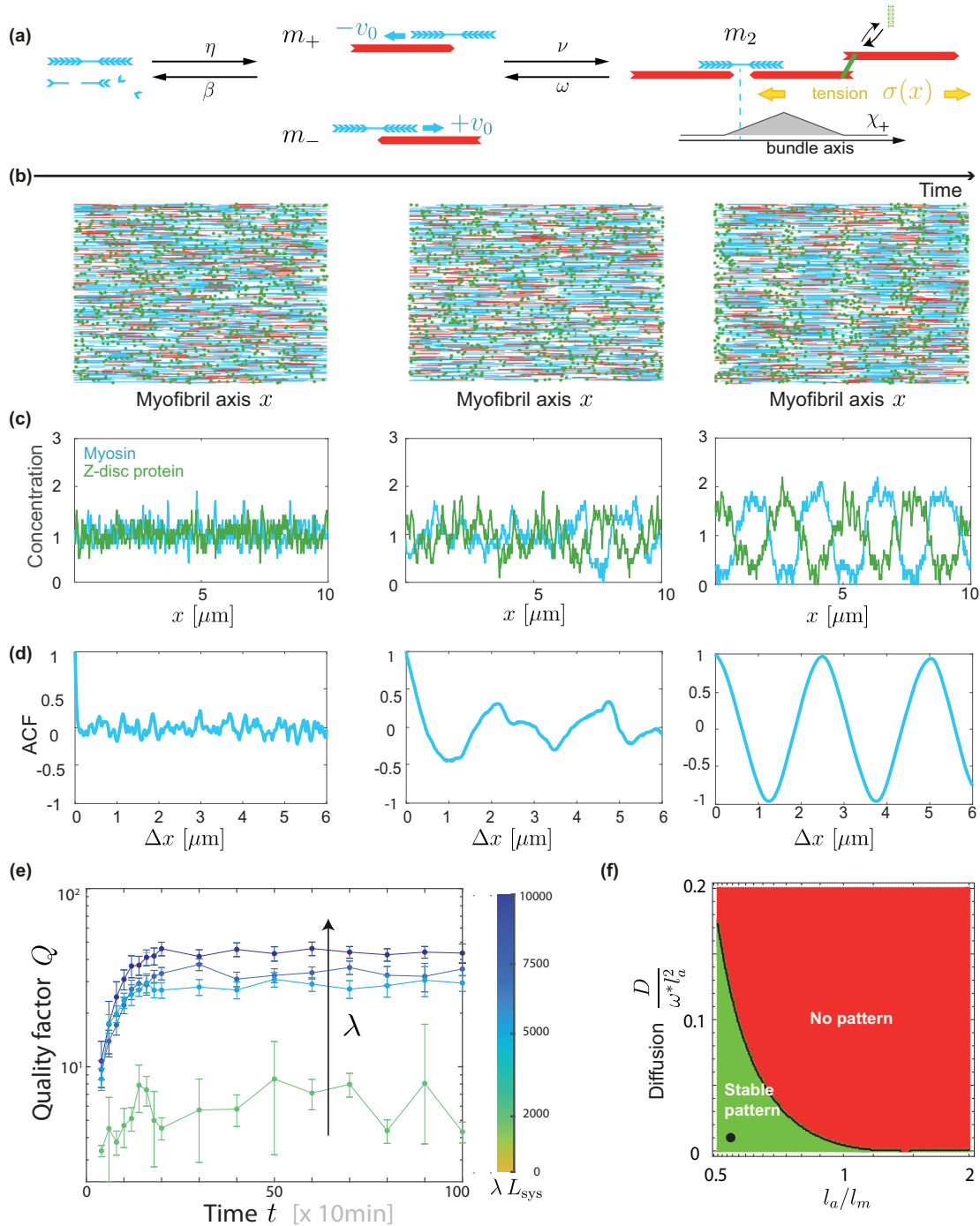
FIG. 4. Pattern formation by tension-responsive catch bonds. (a) Tension-driven myofibrillogenesis: Bipolar myosin filaments can attach to polar actin filaments in different configurations labeled m_+, m_-, and m_2 distinguished in Eqs. (5) and (6). Single-bound myosin with concentrations $m_\pm(x)$ are attached to actin filaments of only one polarity (referred to as + and −, respectively), and move towards the respective plus end with velocity $\mp v_0$. Double-bound myosin filaments with concentration $m_2(x)$ are attached simultaneously to actin filaments of opposite polarity, and thus do not move, but generate active tension $\sigma(x)$. The Z-disk protein α-actinin is a catch-bond, i.e., its unbinding rate from actin decreases with increased tension. Together, this defines a second nonlocal interaction from myosin to Z-disk proteins. (b) Snapshots of agent-based simulations of the mathematical model II at different simulation times ($t = 0$, 2, 100). Simulations of model II in Eqs. (5)–(7) were performed in one space dimension, and visualized in two dimensions for clarity with double-bound myosin (blue), Z-disk protein (green), and polar actin filaments (red). (c) Corresponding concentration profiles $m_2(x)$ and $z(x)$ at time points $t = 0$, 2, 100 for double-bound myosin (blue) and Z-disk protein (green). (d) Corresponding ACFs for these concentration profiles. (e) Quality factor Q characterizing the regularity of periodic myosin patterns as function of time t for different values of the number-density parameter λ scaling small-number fluctuations (mean $\pm$ s.e.m., $n = 10$ simulation runs). (f) Phase diagram showing regimes of stable patten formation as function of the relative length l_a/l_m of actin filaments, and the effective diffusion coefficient D of myosin filaments with $\omega^* = \omega(m_2^*)$. Parameters (b)–(d): $\lambda = 5000/L_{\rm sys}$. For detailed list of model parameters, see Table S2 in the SM [39].

proteins $z(x)$:

$$\frac{\partial m_\pm}{\partial t} = D\nabla^2 m_\pm \mp v_0 \boldsymbol{\nabla} m_\pm - \beta m_\pm + \eta - \nu\, m_\pm + \omega\, m_2,$$

$$(5)$$

$$\frac{\partial m_2}{\partial t} = D\nabla^2 m_2 + \nu(m_+ + m_-) - 2\omega\, m_2, \qquad (6)$$

$$\frac{\partial z}{\partial t} = D\nabla^2 z - \beta_z(\sigma) z + \eta_z. \qquad (7)$$

Equations (5)–(7) account for random motion modeled as effective diffusion with diffusion coefficient D, as well as unbinding and binding of myosin and Z-disk proteins to the scaffold of aligned actin filaments. Additionally, Eq. (5) contains a drift term that accounts for the active displacement of single-bound myosin along actin filaments. Single-bound myosin filaments that bind to a second actin filament of opposite polarity enter as a loss term $-\nu m_\pm$ in Eq. (5) for $m_\pm(x)$, but as a gain term in Eq. (6) for $m_2(x)$; analogously, ωm_2 accounts for double-bound myosin filaments that unbind from actin filaments of one polarity, but stay bound to actin filaments of the opposite polarity; see Fig. 4(a).

Analogous to model I, the binding and unbinding rate parameters $\eta = \eta(z)$, $\nu = \nu(m_2)$, $\omega = \omega(m_2)$, $\eta_z = \eta_z(z)$ additionally depend on the local concentrations of myosin and Z-disk proteins, describing steric repulsion effects and autocatalytic binding; see the SM [39] for details.

The effective unbinding rate β for single-bound myosin accounts for the fact that a single-bound myosin filament falls off the actin filament once it reaches its plus end.

Linear stability analysis of Eqs. (5)–(7) reveals again parameter regimes, for which the homogeneous steady state is unstable, and regular periodic patterns with alternating peaks of bound myosin and Z-disk proteins form.

Likewise, agent-based simulations, analogous to those for model I, reveal spontaneous sorting of myosin filaments and Z-disk proteins; see Fig. 4(b) as well as Fig. 4(c) for concentration profiles at different simulation times. Amplitudes and wavelengths of emergent periodic patterns are comparable to those of model I. The wavelength of patterns is now set by the length of myosin and actin filaments.

From the autocorrelation functions of concentration profiles shown in Fig. 4(d), we obtain again a quality factor that characterizes the regularity of patterns; see Fig. 4(e). As expected, the quality factor increases with increasing number-density parameter λ, yet, as an important difference with model I, we find that no periodic patterns emerge if λ is too low with $\lambda \lesssim 1000/L_{sys}$.

Similar to small-number fluctuations, stochastic motion of molecules characterized by the effective diffusion coefficient D suppresses patterns; see Fig. 4(f).

We emphasize that models I and II represent physically distinct mechanisms yet share a similar feedback logic. Correspondingly, they display a similar pattern-forming behavior. Model II is slightly less robust than model I, reflected by smaller quality factors, and a collapse of periodic patterns already at intermediate values of the number-density parameter λ. Myofibrillogenesis *in vivo* likely uses a combination of models I and II.

III. DISCUSSION

Here we presented data on the early stages of myofibrillogenesis in *Drosophila melanogaster*, revealing a sequential ordering of the sarcomere components α-actinin, actin, muscle-specific myosin heavy chain, and the titin homologue Sallimus. Quantitative analysis using a new, tracking-free algorithm to compute auto- and cross-correlation functions shows that α-actinin, myosin, and Sallimus establish periodic patterns with alternating localization first, while actin follows later.

Based on these observations, we propose two putative models of sarcomere self-assembly, which we formulate as minimal mathematical models. We propose that myosin and Z-disk proteins bind and unbind to a scaffold of parallel aligned, but not yet polarity-sorted actin filaments, establishing periodic patterns as a consequence of autocatalytic attachment, mutual interactions, and a negative feedback loop reflecting steric repulsion.

Our model I includes nonlocal interactions mediated by extended myosin filaments and the giant protein titin/Sallimus, which binds to bipolar myosin filaments at its C-terminus and is supposed to recruit Z-disk proteins such as α-actinin at its N-terminus. We thus assume in model I that Sallimus is incorporated already in its extended configuration, as has been shown to be the case in mature sarcomeres [5]. Sallimus would become mechanically strained later, possibly as consequence of an increase in sarcomere length. Intriguingly, previous experiments with genetically engineered titin demonstrated that varying titin length directly affects sarcomere length [27–29]. Decreasing titin length reduces the length scale of nonlocal interaction in our model I, which decreases the emergent sarcomere length in an almost linear fashion.

A modified model I, in which the roles of myosin and Z-disk proteins are flipped, where Z-disk proteins exert a nonlocal interaction on myosin, e.g., by recruiting Sallimus, which then stabilizes bound myosin, while myosin disfavors binding of Z-disk proteins due to steric hindrance, would yield analogous patterns by symmetry.

In a second model (model II), a similar nonlocal interaction results from the catch-bond behavior of Z-disk proteins such as α-actinin [33,34] in response to local tension generated by myosin motor activity. Analogously, Z-disk protein complexes (e.g., Zasp52/α-actinin) or myosin itself could act as tension sensors [16].

Using agent-based simulations, we demonstrate the robustness of both mathematical models to small-number fluctuations, with a breakdown of pattern formation below a critical number density of about 50 myosin filaments per sarcomere unit in model I, but about 500 myosin filaments in model II.

While model II accounts for the experimental observation that myofibrillogenesis requires mechanical tension [6,7,10–12], model I reproduces the observed decrease of sarcomere size upon genetic shortening of titin [27–29]. *In vivo* myofibrillogenesis could exploit a combination of model I and II, which may explain the high robustness of this process *in vivo*.

Our proposed feedback scheme does not represent a classical Turing mechanism with diffusion-driven instability [49]; instead, patterns emerge from nonlocal interactions, formally

similar to previous work by Kondo *et al.* on zebrafish stripe patterns [50].

Based on data, our models assume that periodic actin patterns will become established later. A simple mechanism for subsequent actin ordering would be continuous actin turn-over, whereby new actin filaments become preferentially nucleated at nascent Z-disks (see also Fig. S16 in the SM [39]). Additionally, ectopic actin filaments that are not sufficiently cross-linked by Z-disk proteins may be moved by myosin motor activity and eventually either become captured at a Z-disk or depolymerize. In particular, motion of these actin filaments may cause actin buckling, which could trigger accelerated depolymerization [51–53]; see also previous studies that observe accelerated actin turnover as result of myosin activity [54–56]. Thus, preferential nucleation of new actin filaments at periodically positioned Z-disk precursors would ensure correct actin polarity within emerging sarcomeres, while the original scaffold of actin filaments with random polarity would be steadily remodeled and partially disassembled.

While it would be naïve to assume that myofibrillogenesis proceeds identically in all animals, we conceive that the physical principles proposed here could be conserved. For example, Sanger proposed a premyofibril model of myofibrillogenesis in which nonmuscle myosin establishes periodic patterns first that later become replaced by muscle-specific myosin [57]. It is conceivable that our model may apply to a patterning of nonmuscle myosin and Z-disk proteins. To validate our model, future cryo-electron tomography could assess the length and structural polarity of actin and myosin filaments, as recently done in mature sarcomeres [58,59].

Our minimal mathematical models comprise effective parameters that coarse-grain biophysical parameters. The predicted patterning is robust and largely independent of specific parameter choices. Nonetheless, future fine-grained models should be quantitative and employ measured parameters, of which only some are known to date. Sarcomere assembly is a fast process in arthropods, spanning just 26–32 h APF for the *Drosophila* flight muscle.

In unstriated stress fibers, the length of actin filaments ranges from 0.5–2 μm [60]; the distribution of actin filament length could be similarly disperse in early myofibrils. The length of bipolar myosin filaments in vertebrates equals $l_m \approx$ 1.6 μm in mature sarcomeres [61].

The density of myosin filaments in the cross section of developing myofibrils at 32 h and 48 h APF estimated from electron micrographs equals approximately 150 μm^{-2} [37] corresponding to about 35 myosin filaments per myofibrillar cross section of 0.5 μm diameter [38], or a value $\lambda \sim 150/L_{sys}$ of the number-density parameter in our model. During myofibrillogenesis, myosin expression is upregulated [12], and the number of individual myosin heavy chains per bipolar myosin filament increases with time [38,62], which would correspond to a dynamic increase of an effective value of the number-density parameter λ in our model. Striated stress fibers with as low as 10–30 nonmuscle myosin filaments in each myosin band were observed in cultured fibroblasts [63]. The stoichiometry between actin and myosin filaments was inferred as 3:1 in mature insect flight muscle [64,65]. A sliding speed of nonmuscle myosin of 0.15 μm/min was observed in nascent striated stress fibers [42]; we expect that

the sliding speed v_0 of muscle myosin during myofibril assembly stages is closer to this value than to the maximal speed 6 μm/s of myosin filaments measured in mature fast skeletal muscle [66]. In mature myofibrils, each bipolar myosin filament (thick filament) contains 600 myosin motor heads [67], each of which can generate a maximal force of approximately 1 pN, though at low duty ratio <0.1 [66,68–70]. Each bipolar myosin filament is thus estimated to generate tensile forces in the range 1–10 pN [71].

Experiments in the actin cortex of HeLa cells indicate a critical tension of the catch-bond α-actinin of $\gamma_c \approx 1$ nN/μm [33]. Assuming a cortical thickness of $h = 200$ nm with actin network meshsize $a = 50$ nm, this value would correspond to a molecular force of $a^2\gamma_c/h \approx 10$ pN.

FRAP experiments in beating cardiomyocytes revealed two actin populations with fast ($\sim$1 min, 25%) and slow (>30 min, 75%) turnover, respectively [54]. Likewise, FRAP experiments in cultured quail myotubes indicated distinct populations of actin filaments and various Z-disk proteins including α-actinin, with typical turnover times $\sim$10 min [72]. For comparison, FRAP experiments in stress fibers indicate turnover rates of $\approx$0.5 min^{-1} for actin and $\approx$3 min^{-1} for α-actinin [73].

The observation of two distinct actin populations with different turnover times in FRAP experiments of nascent myofibrils and stress fibers [54,73] may reflect the initial scaffold of weakly cross-linked actin filaments and a subsequent population of anchored actin filaments that may have been polymerized *de novo* at nascent Z-disks as proposed here.

Generally, the exchange dynamics of sarcomeric components seems to slow down during myofibril maturation [72]. Turnover of titin/Sallimus in mature *Drosophila* larval muscle was slow with turnover times >30 min [26], consistent with previous results for titin turnover in cultured mouse myocytes of several hours [74].

Assuming a value of 0.1 min^{-1} for binding and unbinding rates in our mathematical model would convert the time for the formation of periodic sarcomeric patterns from 20 simulation time units to 3 h, which is at least consistent with observations. Similarly, myosin speed v_0 in model II would correspond to 0.2 μm/min.

Our mathematical models make testable predictions. For instance, filament lengths and interaction length scales set sarcomere size. A partial knockdown of myosin, Z-disk proteins, or actin reduces the regularity of sarcomeric patterns and leads to a complete loss of patterns beyond a characteristic knockdown strength, consistent with experimental data [16,44].

In conclusion, we have proposed two putative mechanisms of sarcomere self-assembly and have tested them through two mathematical models, which are both able to produce the characteristic sarcomeric pattern. These models can guide future experiments addressing partial loss of function of different sarcomeric components or reduction in myosin forces.

IV. MICROSCOPY METHODS

To investigate polarity sorting of actin filaments, we examined the actin-capping protein Tropomodulin (Tmod), which is highly specific to the minus ends of actin filaments [75], using endogenously tagged GFP lines from [76,77].

Tmod-GFP/+ pupae were dissected in PBS and then immediately mounted on a slide and examined (without tissue fixation) under the confocal microscope at 32 h and 48 h APF (Tmod-GFP fly stock BDSC no. 59303).

Drosophila Mhc[*weeP26*](*Mhc*-GFP) larvae were grown at 27 °C and collected at the time of puparium formation (white-colored pupae). Pupae were then maintained at 27 °C for at least 22 h and up to 32 h after puparium formation (APF), which corresponds to the time window of sarcomere assembly in *Drosophila* indirect flight muscles at that temperature [6,62]. At each time point (22, 24, 26, 28, 30 and 32 h APF), pupae were fixed with 4% paraformaldehyde in PBS-T (PBS + 0.3% Triton X-100) for 30 min at room temperature. Pupae were then washed twice in PBS-T for at least 10 min, and, still in PBS-T, thoraxes were dissected and cut in half as described in [6] to visualize indirect flight muscles. Staining was done in PBS-T: actin was labeled with Phalloidin Alexa-568 (Thermo Fisher, 1:500), and titin/Sallimus and *α*-actinin were labeled with the fluorescently labeled nanobodies [26] Sls-Nano2-DyLight405 and Actn-Nano62-Atto647, respectively. Samples were stained overnight at 4 °C, then washed three times (3 × 10 min) in PBS-T and mounted in SlowFade Gold Antifade (Thermo Fisher). Samples were imaged with a Zeiss LSM880 confocal microscope using an 100× objective in AiryScan mode (R-S), with a 2.5× zoom. We processed the Airyscan raw data within the software ZEN using the default (automatically calculated) strength value.

The experiment was performed twice and images were acquired from in total seven different animals. Staining for *α*-actinin had been added in the second experimental run, which corresponds to four different animals.

---

[1] S. B. Lemke and F. Schnorrer, Mechanical forces during muscle development, Mech. Dev. **144**, 92 (2017).

[2] A. F. Huxley and R. Niedergerke, Structural changes in muscle during contraction: Interference microscopy of living muscle fibres, Nature (London) **173**, 971 (1954).

[3] H. E. Huxley, The mechanism of muscular contraction, Sci. Am. **213**, 18 (1965).

[4] W. A. Linke, Titin gene and protein functions in passive and active muscle, Annu. Rev. Physiol. **80**, 389 (2018).

[5] F. Schueder, P. Mangeol, E. H. Chan, R. Rees, J. Schünemann, R. Jungmann, D. Görlich, and F. Schnorrer, Nanobodies combined with DNA-paint super-resolution reveal a staggered titin nano-architecture in flight muscles, eLife **12**, e79344 (2023).

[6] M. Weitkunat, A. Kaya-Çopur, S. W. Grill, and F. Schnorrer, Tension and force-resistant attachment are essential for myofibrillogenesis in *Drosophila* flight muscle, Curr. Biol. **24**, 705 (2014).

[7] A. Chopra, M. L. Kutys, K. Zhang, W. J. Polacheck, C. C. Sheng, R. J. Luu, J. Eyckmans, J. T. Hinson, J. G. Seidman, C. E. Seidman *et al.*, Force generation via *β*-cardiac myosin, titin, and *α*-actinin drives cardiac sarcomere assembly from cell-matrix adhesions, Dev. Cell **44**, 87 (2018).

[8] T. Tucholski, W. Cai, Z. R. Gregorich, E. F. Bayne, S. D. Mitchell, S. J. McIlwain, W. J. de Lange, M. Wrobbel, H. Karp, Z. Hite *et al.*, Distinct hypertrophic cardiomyopathy genotypes result in convergent sarcomeric proteoform profiles revealed by top-down proteomics, Proc. Natl. Acad. Sci. USA **117**, 24691 (2020).

[9] D. S. Herman, L. Lam, M. R. Taylor, L. Wang, P. Teekakirikul, D. Christodoulou, L. Conner, S. R. DePalma, B. McDonough, E. Sparks *et al.*, Truncations of titin causing dilated cardiomyopathy, N. Engl. J. Med. **366**, 619 (2012).

[10] N. M. Luis and F. Schnorrer, Mechanobiology of muscle and myofibril morphogenesis, Cells Dev. **168**, 203760 (2021).

[11] Q. Mao, A. Acharya, A. Rodríguez-delaRosa, F. Marchiano, B. Dehapiot, Z. Al Tanoury, J. Rao, M. Díaz-Cuadros, A. Mansur, E. Wagner *et al.*, Tension-driven multi-scale self-organisation in human iPSC-derived muscle fibers, eLife **11**, e76649 (2022).

[12] S. Majkut, T. Idema, J. Swift, C. Krieger, A. Liu, and D. E. Discher, Heart-specific stiffening in early embryos parallels matrix and myosin expression to optimize beating, Curr. Biol. **23**, 2434 (2013).

[13] J. W. Sanger, J. Wang, B. Holloway, A. Du, and J. M. Sanger, Myofibrillogenesis in skeletal muscle cells in zebrafish, Cell Motil. Cytoskeleton **66**, 556 (2009).

[14] A. M. Fenix, A. C. Neininger, N. Taneja, K. Hyde, M. R. Visetsouk, R. J. Garde, B. Liu, B. R. Nixon, A. E. Manalo, J. R. Becker *et al.*, Muscle-specific stress fibers give rise to sarcomeres in cardiomyocytes, eLife **7**, e42144 (2018).

[15] H. Holtzer, T. Hijikata, Z. X. Lin, Z. Q. Zhang, S. Holtzer, F. Protasi, C. Franzini-Armstrong, and H. L. Sweeney, Independent assembly of 1.6 μm long bipolar Mhc filaments and I-Z-I bodies, Cell Struct. Funct. **22**, 83 (1997).

[16] Y. Rui, J. Bai, and N. Perrimon, Sarcomere formation occurs by the assembly of multiple latent protein complexes, PLoS Genet. **6**, e1001208 (2010).

[17] E. Ehler, B. M. Rothen, S. P. Hämmerle, M. Komiyama, and J. C. Perriard, Myofibrillogenesis in the developing chicken heart: Assembly of Z-disk, M-line and the thick filaments, J. Cell Sci. **112**, 1529 (1999).

[18] A. Zemel and A. Mogilner, Expansion and polarity sorting in microtubule-dynein bundles, Prog. Theor. Phys. Suppl. **173**, 17 (2008).

[19] N. Yoshinaga, J. F. Joanny, J. Prost, and P. Marcq, Polarity patterns of stress fibers, Phys. Rev. Lett. **105**, 238103 (2010).

[20] B. M. Friedrich, E. Fischer-Friedrich, N. S. Gov, and S. A. Safran, Sarcomeric pattern formation by actin cluster coalescence, PLoS Comput. Biol. **8**, e1002544 (2012).

[21] A. Zemel and A. Mogilner, Motor-induced sliding of microtubule and actin bundles, Phys. Chem. Chem. Phys. **11**, 4821 (2009).

[22] S. Tojkander, G. Gateva, G. Schevzov, P. Hotulainen, P. Naumanen, C. Martin, P. W. Gunning, and P. Lappalainen, A molecular pathway for myosin II recruitment to stress fibers, Curr. Biol. **21**, 539 (2011).

[23] R. Littlefield, A. Almenar-Queralt, and V. M. Fowler, Actin dynamics at pointed ends regulates thin filament length in striated muscle, Nat. Cell Biol. **3**, 544 (2001).

[24] C. C. Gregorio, H. Granzier, H. Sorimachi, and S. Labeit, Muscle assembly: A titanic achievement?, Curr. Opin. Cell Biol. **11**, 18 (1999).

[25] P. F. M. van der Vens, J. W. Bartsch, M. Gautel, H. Jockusch, and D. Furst, A functional knock-out of titin results in defective myofibril assembly, J. Cell Sci. **113**, 1405 (2000).

[26] V. Loreau, R. Rees, E. H. Chan, W. Taxer, K. Gregor, B. Mußil, C. Pitaval, N. M. Luis, P. Mangeol, F. Schnorrer, and D. Görlich, A nanobody toolbox to investigate localisation and dynamics of *Drosophila* titins and other key sarcomeric proteins, eLife **12**, e79343 (2023).

[27] L. Tskhovrebova and J. Trinick, Titin: properties and family relationships, Nat. Rev. Mol. Cell Biol. **4**, 679 (2003).

[28] A. Brynnel, Y. Hernandez, B. Kiss, J. Lindqvist, M. Adler, J. Kolb, R. Van der Pijl, J. Gohlke, J. Strom, J. Smith *et al.*, Downsizing the molecular spring of the giant protein titin reveals that skeletal muscle titin determines passive stiffness and drives longitudinal hypertrophy, eLife **7**, e40532 (2018).

[29] H. L. Granzier, K. R. Hutchinson, P. Tonino, M. Methawasin, F. W. Li, R. E. Slater, M. M. Bull, C. Saripalli, C. T. Pappas, C. C. Gregorio *et al.*, Deleting titin's I-band/A-band junction reveals critical roles for titin in biomechanical sensing and cardiac function, Proc. Natl. Acad. Sci. USA **111**, 14589 (2014).

[30] V. Wollrab, J. M. Belmonte, L. Baldauf, M. Leptin, F. Nédeléc, and G. H. Koenderink, Polarity sorting drives remodeling of actin-myosin networks, J. Cell Sci. **132**, (2019).

[31] A. Zumdieck, K. Kruse, H. Bringmann, A. A. Hyman, and F. Jülicher, Stress generation and filament turnover during actin ring constriction, PLoS ONE **2**, e696 (2007).

[32] T. Luo, K. Mohan, P. A. Iglesias, and D. N. Robinson, Molecular mechanisms of cellular mechanosensing, Nat. Mater. **12**, 1064 (2013).

[33] K. Hosseini, L. Sbosny, I. Poser, and E. Fischer-Friedrich, Binding dynamics of α-actinin-4 in dependence of actin cortex tension, Biophys. J. **119**, 1091 (2020).

[34] Y. Mulla, M. J. Avellaneda, A. Roland, L. Baldauf, W. Jung, T. Kim, S. J. Tans, and G. H. Koenderink, Weak catch bonds make strong networks, Nat. Mater. **21**, 1019 (2022).

[35] V. Ruffine, A. Hartmann, A. Frenzel, M. Schlierf, and E. Fischer-Friedrich, Twofold mechanosensitivity ensures actin cortex reinforcement upon peaks in mechanical tension, Adv. Phys. Res. **2**, 2300046 (2023).

[36] K. Dasbiswas, S. Hu, F. Schnorrer, S. A. Safran, and A. D. Bershadsky, Ordering of myosin II filaments driven by mechanical forces: Experiments and theory, Philos. Trans. R. Soc. B **373**, 20170114 (2018).

[37] O. Loison, M. Weitkunat, A. Kaya-Çopur, C. Nascimento Alves, T. Matzat, M. L. Spletter, S. Luschnig, S. Brasselet, P.-F. Lenne, and F. Schnorrer, Polarization-resolved microscopy reveals a muscle myosin motor-independent mechanism of molecular actin ordering during sarcomere maturation, PLoS Biol. **16**, e2004718 (2018).

[38] M. L. Spletter, C. Barz, A. Yeroslaviz, X. Zhang, S. B. Lemke, A. Bonnard, E. Brunner, G. Cardone, K. Basler, B. H. Habermann *et al.*, A transcriptomics resource reveals a transcriptional transition during ordered sarcomere morphogenesis in flight muscle, eLife **7**, e34058 (2018).

[39] See Supplemental Material at http://link.aps.org/supplemental/10.1103/PRXLife.2.013002 for additional details on experimental methods, image analysis, and stability analysis of mathematical models.

[40] S. B. Lemke, T. Weidemann, A.-L. Cost, C. Grashoff, and F. Schnorrer, A small proportion of talin molecules transmit forces at developing muscle attachments in vivo, PLoS Biol. **17**, e3000057 (2019).

[41] D. Chereau, M. Boczkowska, A. Skwarek-Maruszewska, I. Fujiwara, D. B. Hayes, G. Rebowski, P. Lappalainen, T. D. Pollard, and R. Dominguez, Leiomodin is an actin filament nucleator in muscle cells, Science **320**, 239 (2008).

[42] S. Hu, K. Dasbiswas, Z. Guo, Y. H. Tee, V. Thiagarajan, P. Hersen, T. L. Chew, S. A. Safran, R. Zaidel-Bar, and A. D. Bershadsky, Long-range self-organization of cytoskeletal myosin II filament stacks, Nat. Cell Biol. **19**, 133 (2017).

[43] Y. Jiu, R. Kumari, A. M. Fenix, N. Schaible, X. Liu, M. Varjosalo, R. Krishnan, D. T. Burnette, and P. Lappalainen, Myosin-18B promotes the assembly of myosin II stacks for maturation of contractile actomyosin bundles, Curr. Biol. **29**, 81 (2019).

[44] C. J. Beall, M. A. Sepanski, and E. A. Fyrberg, Genetic dissection of *Drosophila* myofibril formation: Effects of actin and myosin heavy chain null alleles., Genes Dev. **3**, 131 (1989).

[45] A. Katzemich, N. Kreisköther, A. Alexandrovich, C. Elliott, F. Schöck, K. Leonard, J. Sparrow, and B. Bullard, The function of the M-line protein obscurin in controlling the symmetry of the sarcomere in the flight muscle of *Drosophila*, J. Cell Sci. **125**, 4170 (2012).

[46] A. Sponga, J. L. Arolas, T. C. Schwarz, C. M. Jeffries, A. Rodriguez Chamorro, J. Kostan, A. Ghisleni, F. Drepper, A. Polyansky, E. De Almeida Ribeiro *et al.*, Order from disorder in the sarcomere: FATZ forms a fuzzy but tight complex and phase-separated condensates with α-actinin, Sci. Adv. **7**, eabg7653 (2021).

[47] Z. Orfanos, K. Leonard, C. Elliott, A. Katzemich, B. Bullard, and J. Sparrow, Sallimus and the dynamics of sarcomere assembly in *Drosophila* flight muscles, J. Mol. Biol. **427**, 2151 (2015).

[48] R. Ma, G. S. Klindt, I. H. Riedel-Kruse, F. Jülicher, and B. M. Friedrich, Active phase and amplitude

fluctuations of flagellar beating, Phys. Rev. Lett. **113**, 048101 (2014).

[49] A. M. Turing, The chemical basis of morphogenesis, Philos. Trans. R. Soc. **237**, 37 (1952).

[50] S. Kondo, M. Watanabe, and S. Miyazawa, Studies of Turing pattern formation in zebrafish skin, Philos. Trans. R. Soc. A **379**, 20200274 (2021).

[51] M. P. Murrell and M. L. Gardel, F-actin buckling coordinates contractility and severing in a biomimetic actomyosin cortex, Proc. Natl. Acad. Sci. USA **109**, 20820 (2012).

[52] M. Lenz, T. Thoresen, M. L. Gardel, and A. R. Dinner, Contractile units in disordered actomyosin bundles arise from F-actin buckling, Phys. Rev. Lett. **108**, 238107 (2012).

[53] M. Soares e Silva, M. Depken, B. Stuhrmann, M. Korsten, F. C. MacKintosh, and G. H. Koenderink, Active multistage coarsening of actin networks driven by myosin motors, Proc. Natl. Acad. Sci. USA **108**, 9408 (2011).

[54] A. Skwarek-Maruszewska, P. Hotulainen, P. K. Mattila, and P. Lappalainen, Contractility-dependent actin dynamics in cardiomyocyte sarcomeres, J. Cell Sci. **122**, 2119 (2009).

[55] Y. Aratyn-Schaus, P. W. Oakes, and M. L. Gardel, Dynamic and structural signatures of lamellar actomyosin force generation, Mol. Biol. Cell **22**, 1330 (2011).

[56] L. Haviv, N. Gov, Y. Ideses, and A. Bernheim-Groswasser, Thickness distribution of actin bundles *in vitro*, Eur. Biophys. J. **37**, 447 (2008).

[57] J. W. Sanger, S. Kang, C. C. Siebrands, N. Freeman, A. Du, J. Wang, A. L. Stout, and J. M. Sanger, How to build a myofibril, J. Muscle Res. Cell Motil. **26**, 343 (2006).

[58] Z. Wang, M. Grange, T. Wagner, A. L. Kho, M. Gautel, and S. Raunser, The molecular basis for sarcomere organization in vertebrate skeletal muscle, Cell **184**, 2135 (2021).

[59] Z. Wang, M. Grange, S. Pospich, T. Wagner, A. L. Kho, M. Gautel, and S. Raunser, Structures from intact myofibrils reveal mechanism of thin filament regulation through nebulin, Science **375**, eabn1934 (2022).

[60] L. P. Cramer, M. Siebert, and T. J. Mitchison, Identification of novel graded polarity actin filament bundles in locomoting heart fibroblasts: Implications for the generation of motile force, J. Cell Biol. **136**, 1287 (1997).

[61] D. S. Gokhin and V. M. Fowler, Thin filament architecture in skeletal muscle: A two-segment model, Nat. Rev. Mol. Cell Biol. **14**, 113 (2013).

[62] Z. Orfanos and J. C. Sparrow, Myosin isoform switching during assembly of the *Drosophila* flight muscle thick filament lattice, J. Cell Sci. **126**, 139 (2013).

[63] L. J. Peterson, Z. Rajfur, A. S. Maddox, C. D. Freel, Y. Chen, M. Edlund, C. Otey, and K. Burridge, Simultaneous stretching

and contraction of stress fibers in vivo, Mol. Biol. Cell **15**, 3497 (2004).

[64] H. Iwamoto, Y. Nishikawa, J. Wakayama, and T. Fujisawa, Direct x-ray observation of a single hexagonal myofilament lattice in native myofibrils of striated muscle, Biophys. J. **83**, 1074 (2002).

[65] K. A. Taylor, H. Rahmani, R. J. Edwards, and M. K. Reedy, Insights into actin-myosin interactions within muscle from 3D electron microscopy, Int. J. Mol. Sci. **20**, 1703 (2019).

[66] J. Howard, *Mechanics of Motor Proteins and the Cytoskeleton* (Sinauer, Sunderland, MA, 2002).

[67] J. Davis, Assembly processes in vertebrate skeletal thick filament formation, Annu. Rev. Biophys. Biophys. Chem. **17**, 217 (1988).

[68] P. C. Geiger, M. J. Cody, R. L. Macken, and G. C. Sieck, Maximum specific force depends on myosin heavy chain content in rat diaphragm muscle fibers, J. Appl. Physiol. **89**, 695 (2000).

[69] J. Robert-Paganin, O. Pylypenko, C. Kikuti, H. L. Sweeney, and A. Houdusse, Force generation by myosin motors: A structural perspective, Chem. Rev. **120**, 5 (2020).

[70] Y. Takagi, E. E. Homsher, Y. E. Goldman, and H. Shuman, Force generation in single conventional actomyosin complexes under high dynamic load, Biophys. J. **90**, 1295 (2006).

[71] A. F. Huxley and R. M. Simmons, Proposed mechanism of force generation in striated muscle, Nature (London) **233**, 533 (1971).

[72] J. Wang, J. M. Sanger, and J. W. Sanger, Differential effects of latrunculin-A on myofibrils in cultures of skeletal muscle cells: Insights into mechanisms of myofibrillogenesis, Cell Motil. Cytoskeleton **62**, 35 (2005).

[73] P. Hotulainen and P. Lappalainen, Stress fibers are generated by two distinct actin assembly mechanisms in motile cells, J. Cell Biol. **173**, 383 (2006).

[74] K. da Silva Lopes, A. Pietas, M. H. Radke, and M. Gotthardt, Titin visualization in real time reveals an unexpected level of mobility within and between sarcomeres, J. Cell Biol. **193**, 785 (2011).

[75] S. Szikora, T. Gajdos, T. Novák, D. Farkas, I. Földi, P. Lenart, M. Erdélyi, and J. Mihály, Nanoscopy reveals the layered organization of the sarcomeric H-zone and I-band complexes, J. Cell Biol. **219**, e201907026 (2020).

[76] S. Nagarkar-Jaiswal, P.-T. Lee, M. E. Campbell, K. Chen, S. Anguiano-Zarate, M. Cantu Gutierrez, T. Busby, W.-W. Lin, Y. He, K. L. Schulze *et al.*, A library of MiMICs allows tagging of genes and reversible, spatial and temporal knockdown of proteins in *Drosophila*, eLife **4**, e05338 (2015).

[77] A. Schmidt, L. Li, Z. Lv, S. Yan, and J. Großhans, Dia- and Rok-dependent enrichment of capping proteins in a cortical region, J. Cell Sci. **134**, jcs258973 (2021).